Nanoscale

PAPER

View Article Online
View Journal | View Issue

Cite this: *Nanoscale*, 2018, **10**, 1845

Self-assembled thermoresponsive nanostructures of hyaluronic acid conjugates for osteoarthritis therapy†

Pierre Maudens,[a] Sophie Meyer,[a] Christian Alexander Seemayer,[b] Olivier Jordan[a] and Eric Allémann *[a]

Received 12th October 2017,
Accepted 30th November 2017

DOI: 10.1039/c7nr07614b

rsc.li/nanoscale

Under pathological conditions, joints and skin are often affected by an imbalance in the breakdown and production of hyaluronic acid (HA). The unique biochemical and biomechanical properties provided by HA must be restored for the long-term lubrication and cushioning effects. To overcome the inconvenience of repeated injections and the rapid degradation of exogenous HA treatments, HA is conjugated to a thermosensitive polymer, enabling the spontaneous formation of nanoparticles (HA Nano) at body temperature. Three HA Nano preparations are tested for their injectability, sensitivity to enzymatic degradation and cytocompatibility. One of them is delivered *via* subcutaneous and intra-articular injections to healthy mice and tested in a murine osteoarthritis (OA) model. It is found to be biocompatible, to offer a prolonged residence time at the injection site, have the ability to protect cartilage, to reduce pro-inflammatory cytokines and to preserve epiphysis thickness. In this study, HA Nano spontaneously forms nanoparticles at body temperature *in vivo* and is a promising candidate for the next generation of the sustainable/long-lasting treatment of OA and potentially also dermatological conditions.

Introduction

Hydrogels, which are composed of hydrophilic homopolymer or copolymer networks that can swell in water and physiological fluids,[1] are important biomedical materials due to their high water content and tissue-like elasticity. Hyaluronic acid (HA), a natural linear heteropolysaccharide that forms hydrogels, provides a molecular scaffold for many components of the extracellular matrix. HA is typically found in the connective and epithelial tissues of vertebrates. One-third of the total HA mass is renewed over each day throughout the human body.[2] It has a molecular weight ranging from 10^5 to 10^7 Da and excellent viscoelasticity properties.[3]

HA is suitable for a broad spectrum of applications in medicines, cosmetics, and nutraceuticals.[4,5] HA is particularly known for its role in the lubrication and homeostasis of cartilage after local injection into the joints of patients suffering from osteoarthritis (OA). However, injected HA does not persist for a sufficient amount of time in the human body and is cleared from the implant site because of its low retention due to its degradation by hyaluronidase.[6,7] The invasiveness, risk of infection, inconvenience of repeated HA injections and the frequently insufficient clinical response[8] have spurred research into long-lasting and more efficient formulations. Therefore, the chemical modifications of HA, especially cross-linking modifications, aim to improve the properties of HA.[9]

HA alterations that confer thermosensitivity might help to prolong the *in vivo* lifetime/residence of HA. To this end, the thermoresponsive poly(*N*-isopropylacrylamide) (pNiPAM) polymer might be suitable because of its well-defined sol–gel transition.[10] pNiPAM can introduce physical cross-links *via* the association of hydrophobic domains and *in situ* hydrogel formation.[11,12] Below the lower critical solution temperature (LCST), the hydrophobic *N*-substituted groups of pNiPAM are hydrated by water molecules to form a homogeneous solution. Above the LCST, hydrophobic interactions between the *N*-substituted groups increase, and their strength surpasses their hydration energy, leading to the aggregation of hydrophobic polymer chains.[13,14] Besides, low molecular weight pNiPAM is biocompatible and undergoes renal clearance.[15,16] Previously, thermoreversible HA-pNiPAM hydrogels were formulated for various applications such as tissue engineering and drug delivery systems. Similar to pure pNiPAM, these materials form a hydrogel matrix at body temperature.[17] The

[a]*School of Pharmaceutical Sciences, University of Geneva, University of Lausanne, CH-1211 Geneva 4, Switzerland. E-mail: Eric.Allemann@unige.ch; Tel: +41 22 379 61 48*
[b]*Department of Clinical Science, Idorsia Pharmaceuticals Ltd., CH-4123 Allschwil, Switzerland*

†Electronic supplementary information (ESI) available. See DOI: 10.1039/c7nr07614b

disadvantage of the HA-pNiPAM gel matrices is that they do not provide long-term lubrication or cushioning effects since they are relatively rapidly degraded[18,19] and cleared from the body. Thus, there is a high medical need to design and synthesize new biopolymers that possess a long *in vivo* residence time in the body at the injection site and provide appropriate biomechanical properties while being well tolerated.

The aim of the present study was to synthesize a new injectable HA-pNiPAM physically crosslinked hydrogel that is able to form nanoparticles spontaneously upon a change from room to body temperature and is less sensitive to enzymatic degradation, affording a longer residence time at the injection site, and improving joint treatment and dermatological applications. To this end, different grafting strategies that included (or not) a cyclooctyne linker and/or PEG spacer were evaluated.

Experimental

Synthesis of HA conjugates (HA Nano 1, HA Nano 2 and HA Nano)

Dibenzocyclooctyne (DBCO)-amine was purchased from Sigma-Aldrich (St Louis, MO, USA). DBCO-PEG_4-amine was acquired from Click Chemistry Tools (Scottsdale, AZ, USA). HA (MW: 1.85 MDa) produced by lactic fermentation bacteria on a renewable vegetable substrate was a kind gift from Soliance (Pomacle, France). *N*-(3-Dimethylaminopropyl)-*N*′-ethylcarbodiimide hydrochloride (EDC), *N*-hydroxysuccinimide (NHS), azide-terminated poly(*N*-isopropylacrylamide) (pNiPAM-N_3) (MW: 15 kDa), and amine-terminated poly(*N*-isopropylacrylamide) (pNiPAM-amine) were purchased from Sigma-Aldrich (St Louis, MO, USA). Cyanine 5-azide (Cy5-N_3) was provided by Lumiprobe (Hannover, Germany).

Synthesis of HA Nano 1 (Fig. S1; Scheme 1†)

HA-DBCO (1). HA was solubilized in distilled water at 1% (w/v). After the dissolution of the polymer, EDC was added (0.5 eq. COO^-), and 5 min later, NHS was dissolved (0.5 eq. COO^-) in the solution under magnetic stirring (5 min at 800 RPM). The pH was adjusted to 5.0 using 0.1 M NaOH/HCl, monitored using a Metrohm pH gel electrode (Herisau, Switzerland). The linker DBCO-PEG_4-amine was added (0.5 eq. COO^-) with DMSO for a final volume ratio of 40 : 60, water : DMSO. The reaction was stirred overnight at room temperature and then dialyzed (MWCO: 12–14 000, Spectra/Por® membrane, Spectrum Laboratories, Rancho Dominguez, CA, USA) against 5% (w/v) NaCl 3 times for 3 h each at 900 RPM and then against distilled water 3 times for 3 h each at 900 RPM.

HA Nano 1 (2). To the solution transferred to a balloon, pNiPAM-N_3 (1 eq. DBCO) was added under stirring (2 h at 1500 RPM). HA Nano 1 was dialyzed (MWCO: 25 000, Spectra/Por® membrane) against 5% (w/v) NaCl in distilled water 3 times for 3 h each at 900 RPM and then against distilled water 3 times for 3 h each at 900 RPM, lyophilized (Freeze Dryer Alpha 1–4 LDplus, Christ, Osterode am Harz, Germany) (48 h, 1.5×10^{-1} mbar, −40 °C) and stored at 4 °C.

The structure of the intermediate (1) and the resulting conjugate HA Nano 1 (2) was determined from ^{1}H NMR spectra acquired on a Varian Anova Gemini 300 MHz spectrometer (Palo Alto, CA, USA) at ambient temperature using D_2O as a solvent (Fig. S2†). Because of the overlap of the HA and pNiPAM signals, the degree of substitution (DS) was calculated using the integration ratio of the DBCO protons: HA (δ 2.00 parts per million (ppm)) *versus* DBCO (7.67 ppm) protons was used for the intermediate HA-DBCO, and DBCO (7.67 ppm) *versus* pNiPAM (δ 1.13) protons was used for the final product HA Nano 1.

Synthesis of HA Nano 2–3 (Fig. S1; Scheme 2†)

HA-DBCO (1). HA was dissolved in distilled water at 1% (w/v). After the dissolution of the polymer, EDC was added (HA Nano 2: 0.5 eq. COO^-; HA Nano 3: 1 eq. COO^-), and 5 min later, NHS was dissolved (1 eq. COO^-) under magnetic stirring (5 min at 1200 RPM). The pH was adjusted to 5.0 using NaOH/HCl, monitored using a Metrohm pH gel electrode (Herisau, Switzerland). Then, DBCO-amine was added (HA Nano 2: 0.5 eq. COO^-; HA Nano 3: 1 eq. COO^-) with DMSO to a final volume ratio of 40 : 60, water : DMSO. The reaction was stirred overnight at room temperature. HA Nano 2 was dialyzed (MWCO: 12–14 000, Spectra/Por® membrane) against 5% (w/v) NaCl 3 times for 3 h each at 900 RPM and then against distilled water 3 times for 3 h each at 900 RPM. HA Nano 3 was precipitated with ethanol and lyophilized.

HA Nano 2 (2). To the solution transferred to a balloon, pNiPAM-N_3 (1 eq. DBCO) was added under stirring (2 h at 1500 RPM). HA Nano 2 was dialyzed (MWCO: 25 000, Spectra/Por® membrane) against 5% (w/v) NaCl in distilled water 3 times for 3 h each at 900 RPM and then against distilled water 3 times for 3 h each at 900 RPM and lyophilized before storing at 4 °C.

HA Nano 3 (2). HA-DBCO was redissolved in distilled water at 1% (w/v) and pNiPAM-N_3 (1 eq. DBCO) was added under stirring (2 h at 1200 RPM). The resulting HA Nano 3 was dialyzed (MWCO: 25 000, Spectra/Por® membrane) against 5% (w/v) NaCl in distilled water 3 times for 3 h each at 1500 RPM, precipitated in ethanol, lyophilized and stored at 4 °C. The structures and the DSs of HA Nano 2 and 3 were determined from their ^{1}H NMR spectra in D_2O as described for HA Nano 1.

Synthesis of fluorescent HA Nano 1

HA Nano 1 and a fluorescent dye-azide (Cy5-N_3) were coupled using the same synthetic parameters as those used for HA Nano 1, except that 0.1% (w/w) of Cy5-N_3 was added to the mixture before the addition of pNiPAM-N_3.

Synthesis of fluorescent HA (comparative fluorescent control)

HA and a fluorescent dye-azide (Cy5-N_3) were coupled using the same synthetic parameters as those used for the fluorescent HA Nano 1, except that no pNiPAM-N_3 was added to the mixture.

Synthesis of HA-pNiPAM (comparative control)

A comparative control of HA-pNiPAM without the linker was synthesized using the following method. HA was solubilized in distilled water at 1% (w/v). After the dissolution of the polymer, EDC was added (1 eq. COO^-), and 5 min later, NHS was dissolved (1 eq. COO^-) under magnetic stirring (5 min at 1200 RPM). The pH was adjusted to 5.0 using 0.1 M NaOH/HCl, monitored using a Metrohm pH gel electrode (Herisau, Switzerland), and pNiPAM-amine was added (1 eq. COO^-). The reaction was stirred overnight at room temperature. HA-pNiPAM was dialyzed (MWCO: 25 000, Spectra/Por® membrane) against 5% (w/v) NaCl in distilled water 3 times for 3 h each at 1500 RPM, precipitated in ethanol, lyophilized and stored at 4 °C.

Size and morphology of the conjugate particles

HA conjugates were solubilized in distilled water, and the solutions were then heated to 37 °C in an oven, thus forming nanoparticles. The mean size of the HA nanoparticles formed was determined above the LCST using three methods: scanning electron microscopy (SEM) (JEOL microscope, JSM-7001TA, Tokyo, Japan), dynamic light scattering (DLS) (Nanosizer, Malvern, England) and nanoparticle tracking analysis (NTA) (NanoSight LM10, Malvern, England). The SEM samples were prepared by drying a drop of the formulation on a carbon tape at 37 °C. Afterwards, formulations were coated with a 20 nm gold layer (Leica EM SCD 500, Leica Microsystems GmbH, Wetzlar, Germany) then observed with a scanning electron microscope. The mean particle size was obtained from SEM micrographs by averaging the diameters of 50 particles using ImageJ analysis software, version 1.45s (NIH, Bethesda, MD, USA). A commercial HA formulation containing 1% (w/v) HA was used as a reference (Ostenil®, TRB Chemedica, Geneva, Switzerland).

Injectability

The force injection profile of a syringe filled with HA Nano 1–3 was determined at 20 and 37 °C at a speed of 1 mm s^{-1} on a Texture Analyzer TA.XT. plus (Tracomme AG, Switzerland). A 1 mL BD Micro-Fine™ 29G fixed-needle insulin syringe (later used in this study for the injections into mice) and a 1 mL Norm-Ject® syringe with a 23G needle (generally used for injections into human subjects) were used. The empty syringe, PBS, and commercial HA at 20 °C were used as reference.

Rheology

Rheological measurements were performed on 0.4 mL samples of HA Nano 1 (0.75% (w/v)), HA Nano 2 (0.5% (w/v)), HA Nano 3 (5% (w/v)), and commercial HA. The samples were analyzed using a HAAKE RheoStress 1 with a cone-plate geometry and a 35/2° Ti cone (Vreden, Germany) in a controlled humidity chamber. The viscosity curves of the polymers were acquired under rotation steps at a shear rate ranging from 0.1 s^{-1} to 100 s^{-1} at 20 °C. The LCST was also investigated by the dynamic rheometry moduli G' (elasticity) and G'' (viscosity). G' and G'' were measured from 20 to 37 °C at a heating rate of 1 °C min^{-1} through oscillation steps with a constant frequency of 1 Hz.

Stability assay

HA conjugates (n = 3 per time point) were stored at 4 °C, and the viscosity was recorded over time (days 0, 7 and 30) from rheological measurements, as described above.

Enzymatic degradation

Hyaluronidase type IV from bovine testes was purchased from Sigma-Aldrich (St Louis, MO, USA). The enzymatic degradation of HA Nano 1–3 was assessed using 1 mL of the sample at 0.1% (w/v) with 55 U mL^{-1} hyaluronidase in PBS by DLS (Nanosizer, Malvern, England) over 1 h at 37 °C, over 14 h at 20 °C (no particles detected) and over 0.5 h at 37 °C. To determine the enzymatic degradation, G' and G'' were calculated from rheological measurements performed at 37 °C with a constant frequency of 1 Hz for 16 min, as described above. The enzymatic degradation of commercial HA was determined using 1 mL of the sample at 0.9% (w/v) with 55 U mL^{-1} hyaluronidase in PBS.

pH and zeta potential

The pH was measured using a Metrohm pH gel electrode (Herisau, Switzerland), and the zeta potential was measured using a Zetasizer Nano ZS (Malvern, Worcestershire, UK).

In vitro drug release

To determine the drug release profile from the HA conjugate nanoparticles, the *in vitro* drug release was assessed as follows. Saline solution (0.9% (w/v) NaCl), commercial HA, and the graft polymers HA Nano 1–2 were saturated with the dexamethasone base (0.05, 0.57, 2.52, 2.55 mg mL^{-1}, respectively) at 20 °C. Ten milliliters of each of the previous solutions were dialyzed (MWCO: 1000, Spectra/Por® membrane) against 400 mL of 0.9% (w/v) NaCl for 28 h at 37 °C and 80 RPM. After 28 h, the polymer matrix was hydrolyzed by heating (121 °C) to release the remaining content of dexamethasone, and DMSO was added to a final volume ratio of 1 : 1, water : DMSO. The amount of the drug released at each time point was quantified by reversed-phase UHPLC using a C18 Hypersil Gold column (50/2.1, 1.9 μm bead particle size, Thermo Scientific, Waltham, USA). The mobile phase was composed of 0.1% (v/v) formic acid in water (A) and 0.1% (v/v) trifluoroacetic acid (TFA) in acetonitrile (B), and the following gradient elution sequence was applied at a flow rate of 400 μL min^{-1}: 30–95% A (0–3 min), 95–10% A (3–4 min), 10–30% A (4–4.5 min) and 30% A (4.5–5 min).

Cell viability assay

Viability tests were performed using human synovial fibroblasts isolated from the synovial tissue from one OA patient having signed previously an informed consent (passage 8, n = 3). The permission for the study on human tissues was given by the Central Committee for Ethics in Research of Geneva

University Hospital (CER: 05-007 (05-017)). The cells were plated at a density of 20 000 cells per well in 96-well plates. After 24 h, the HA conjugates (HA Nano 1–2) were solubilized in PBS and then incubated for an additional 24 h at 37 °C. Next, 50 μL of 0.5% MTT solution was added to each well, and the plates were left for 3 h. All wells were incubated for 45 min with 100 μL of DMSO, and the absorbance was measured at 570 nm (8 points per well) on a BioTeK Synergy Mx microplate reader (Winooski, VT, USA).

Skin biocompatibility

All *in vivo* experiments were performed in compliance with the Swiss Federal Law on the protection of animals. The protocols were approved by the cantonal Geneva Authority (GE/148/14). 100 μL of fluorescent HA Nano 1 and HA (1% (w/v)) were subcutaneously injected into the back of healthy C57BL/6J mice (6 weeks of age). At 7 and 21 days post-injection, mice (n = 2–4 per time point), under deep anesthesia, were sacrificed by intra-cardiac puncture and spinal cord dislocation. The injected skin was dissected from the sagittal plane where the cyanine 5 fluorescence was detected using a Maestro M1 imaging system (PerkinElmer, Cambridge Research and Instrumentation Inc., Waltham, MA). After fixing in 4% paraformaldehyde for 24 h and embedding in paraffin, 5 μm sections were cut with a microtome. The sections were stained with hematoxylin and eosin (H&E) or left blank for fluorescence analysis. The semi-quantification of macrophages in the tissue based on histology was performed by a pathologist in a blinded manner from (−) to (+++).

Surgical destabilization of the medial meniscus (DMM) model and histology

DMM surgery was performed on the right knee of 6-week-old male C57BL/6 mice (n = 7 per group). The protocols were approved by the cantonal Geneva Authority (GE/170/14). Ten microliters of 1% (w/v) fluorescent HA and HA Nano 1 were intra-articularly injected on days 7 and 35 after the OA surgery as described[20] and adapted. Briefly, under binoculars, a 5 mm longitudinal incision in the skin was made with a #11 blade at day 0. Then, the joint capsule was opened with a longitudinal incision of 2 mm between the patellar ligament and the medial collateral ligament from the medial tibial plateau with an ultrafine micro-knife with a 5 mm cutting edge (Fine Science Tools, Heidelberg, Germany). Finally, the meniscotibial ligament of the medial meniscus was sectioned. The suture line of the joint capsule was closed with a Vicryl® 4-0 suture, and the skin was closed with a Prolene® 5-0 suture (Ethicon, Somerville, NJ, USA). For the sham group, the ligament was only visualized, not transected and the knee was injected with PBS. At day 63, whole blood was collected for further analysis *via* intra-cardiac puncture under deep anesthesia, and the mice were sacrificed by spinal cord dislocation. The knee joints were fixed in 4% paraformaldehyde for 24 h. Whole joints were decalcified in 10% (w/v) Tris-EDTA for 5 weeks on a shaker. The joints were embedded in paraffin, and 5 μm frontal sections were taken at two levels corresponding to one-third and two-thirds of the depth of the knee from the patella. Slides were stained with Safranin-O/Fast Green (SOFG), Toluidine blue and H&E. The severity of OA was evaluated and scored by a pathologist in a blinded manner from normal (0) to severe (6) according to the Osteoarthritis Research Society International (OARSI) recommendations.[21]

Intravital fluorescence

Intravital fluorescence in mice was assessed during the first 21 days after administration *via* two routes of the injection of fluorescent HA Nano 1 and HA (comparative control): intra-articular injection in an OA model (DMM)[20] and subcutaneous injection in healthy mice. At days 0 (approximately 1 h after injection), 1, 7 and 21, the intravital fluorescence based on the spectrum of cyanine 5 was detected in semi-quantitative observations on a Maestro M1 imaging system (PerkinElmer, Cambridge Research and Instrumentation Inc., Massachusetts). Photomicrographs were analyzed using the ImageJ software following the same procedure (Fire scale, brightness, and contrast: min. 10, max. 280).

Fluorescence microscopy

Unstained paraffin embedded joint and skin tissue sections were analyzed by fluorescence microscopy (filter: DAPI and Cy5) on a Zeiss Axio Scan.Z1 scanner™ (Carl Zeiss, Jena, Germany). Photomicrographs were analyzed using the Zeiss software ZEN (Carl Zeiss, Jena, Germany) following the same procedure (DAPI: black 130, white 500, and gamma 1; Cy5: black 130, white 300, and gamma 1).

Micro-computed tomography (micro-CT)

After sacrifice, the knee joints of the mice were scanned on the same day using micro-CT (Quantum FX, PerkinElmer, Hopkinton, MA, USA) with a voxel size of 10 μm. The X-ray tube voltage was 90 kV, and the current was 88 μA. The software OsiriX Lite (OsiriX Foundation, Geneva, Switzerland) was used to measure the epiphysis thickness from the articular cartilage surface to the epiphyseal line at the center of the medial and lateral tibial epiphysis for all samples. All the samples were analyzed with a window level of 1500 and a window width of 3000.

Multiplex enzyme-linked immunosorbent assay (ELISA)

Freshly collected mouse blood samples were immediately placed into tubes containing 1 mg of ethylenediaminetetraacetic acid dipotassium salt purchased from Sigma-Aldrich (St Louis, MO, USA) and centrifuged at 1000g for 15 min and 10 000g for 10 min at 4 °C. Plasma was isolated and stored at −80 °C until further analysis. The multiplex kit and beads were purchased from Bio-Rad Laboratories, Inc. (Hercules, CA, USA). A multiplex assay was performed on the following OA biomarkers according to the specifications of the manufacturer: interleukin-1β (IL-1β), tumor necrosis factor-α (TNFα), and vascular endothelial growth factor (VEGF). Standard curves were generated for each OA biomarker using the reference cytokine concentrations supplied by the manufacturers.

The raw data were analyzed using Bio-Plex Manager software 6.1 to obtain concentrations in μg mL^{-1}.

Statistical analysis

Data are expressed as mean ± standard deviation (s.d.). The statistical significance of the results was determined using one-way or two-way analysis of variance (ANOVA) and a multiple comparison function (Tukey) in Prism 7.2 (GraphPad) with an alpha level of 0.05. *P* values correspond to $*P < 0.0332$, $**P < 0.0021$, $***P < 0.0002$, and $****P < 0.0001$.

Results and discussion

Synthesis and characterization of the HA conjugates

The green chemistry synthetic routes for the HA conjugates (HA Nano 1, HA Nano 2 and HA Nano 3) are reported in Schemes 1 and 2 (Fig. S1†). First, HA (1.85 MDa) was derivatized in an amidation reaction with a DBCO linker (DBCO-amine or DBCO-PEG_4-amine) and was then reacted with pNiPAM-azide (15 kDa, molecular weight adapted for renal excretion). The structural characteristics of the HA conjugates were investigated by ^1H NMR spectroscopy (Fig. S2†). Advantageously, the aromatic protons of DBCO allowed the calculation of the degree of substitution (DS) of the HA conjugates (Fig. 1f) from their NMR spectra. The NMR data demonstrated the grafting efficacy of the reaction in water–DMSO from the native HA sodium salt used without previous modification.[9] The solubility and steric hindrance of the linker played key roles in the final pNiPAM grafting. The copper-free azide-DBCO "click" reaction offered a new polymeric architecture. As a control, a HA-pNiPAM graft polymer was synthesized without the DBCO linker through reactions with EDC and NHS.

In the presence of the DBCO linker, hydrated nanoparticles spontaneously formed above the LCST (Fig. 1a). In contrast, common HA-pNiPAM, which formed a cross-linked hydrogel, did not form nanoparticles, as evidenced by the SEM data and the inability to detect any particles by DLS or NTA. SEM analysis revealed the morphologies of the nanoparticles formulated with the three HA conjugates after incubation at 37 °C (Fig. 1b–d). The HA Nano 3 nanoparticles (Fig. 1d) were more spherical than the HA Nano 1 and 2 nanoparticles (Fig. 1b and c). The appearance of these spherical aggregates was thought to be related to the higher DS of HA Nano 3. In contrast, the graft polymer HA-pNiPAM, without a DBCO linker (negative control, Fig. 1e), and a commercial HA viscosupplement as a control did not form nanoparticles upon heating. Additionally, SEM, DLS and NTA, used as orthogonal characterization methods, provided specific particle sizes in number (mode interval), intensity, and number (mode), respectively (Fig. 1g).

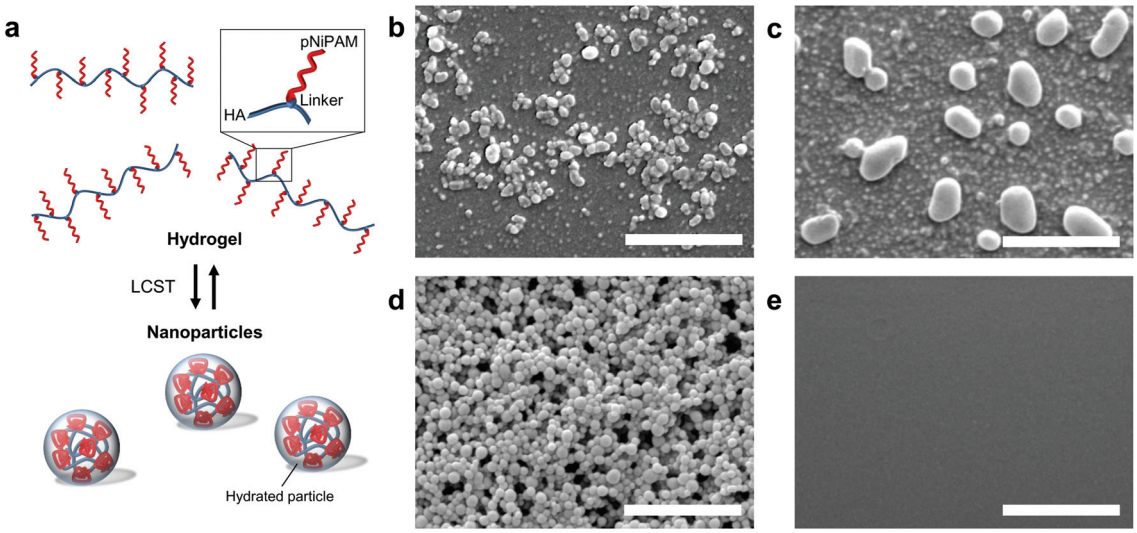

f

	DS % (1 eq. COO^-)
HA Nano 1	4.77
HA Nano 2	3.74
HA Nano 3	7.13

g

	SEM size (nm)	DLS size (nm)	NTA size (nm)
HA Nano 1	203-261; 377-435	239 ± 95	247 ± 27
HA Nano 2	65-84	133 ± 64	122 ± 62
HA Nano 3	88-97	223 ± 55	53 ± 27

Fig. 1 Physicochemical characterization of the nanoparticles formed spontaneously upon heating above the lower critical solution temperature (LCST). a, Schematic representation of the LCST reversible demixing phase transition of the HA conjugates in aqueous solution. Scanning electron micrographs of b, HA Nano 1; c, HA Nano 2; d, HA Nano 3; and e, HA-pNiPAM graft polymer (negative control). Scale bar = 1 μm. f, Degree of substitution (DS) of the 3 HA conjugates. g, Nanoparticle sizes determined by scanning electron microscopy (SEM) (*n* = 3, mode interval in number), dynamic light scattering (DLS) (*n* = 3, mean intensity ± standard deviation (s.d.)), and nanoparticle tracking analysis (NTA) (*n* = 3, mode in number ± s.d.).

In vitro assays: injectability, rheology, and enzymatic degradation

The ease of injection, a critical parameter for joint viscosupplementation and potential dermatological applications,[22] was characterized by the injection profile of the formulations passing through a needle. The HA conjugates at the maximum concentration close to the solubility limit were evaluated with a 23G needle syringe commonly used for clinical viscosupplementation administration *via* intra-articular injections (Fig. 2a and S3†). At the studied concentrations, the initial force (F_i) and the plateau force (F_p) were similar and higher than the final force (F_f). Thus, all formulations were easily injectable (<5 N). To assess the injectability for mouse intra-articular injections, tests with 29G needle-bearing syringes were also conducted at the same polymer concentrations at 20 and 37 °C, which confirmed the ease of injection (Fig. S3†). Furthermore, the rheological analysis of the HA conjugates and the commercial HA used as a control showed non-Newtonian pseudoplastic behaviors (Fig. 2b). Pseudoplastic (rheofluidifying) viscosity, which decreases with increasing shear rate, is a useful property that facilitates injection. The LCST was characterized by a sharp increase in the dynamic storage G' reflecting the elastic behavior of the material and loss moduli G'' representing the viscous behavior as a function of temperature at a heating rate of 1 °C min^{-1} (Fig. 2c). The LCSTs of HA Nano 1–2 were observed at 31–32 °C, in line with the thermosensitive behavior of pNiPAM. For HA Nano 3, a transition phase was observed at 25–26 °C, suggesting a changed LCST based on the environment of the nanoparticles with a higher DS. Corresponding to the observed reversible phase transition, the HA conjugates were hydrogels below their LCST ($G' > G''$) and spontaneously formed nanoparticles above their LCST in the continuous phase while remaining in a gel state ($G' > G''$). This thickening effect (viscosity increase) supports the physical crosslinking of the gel phase that is hydrophobically driven by pNiPAM, concurrent with the nanostructuration revealed by DLS, NTA, and SEM. For further

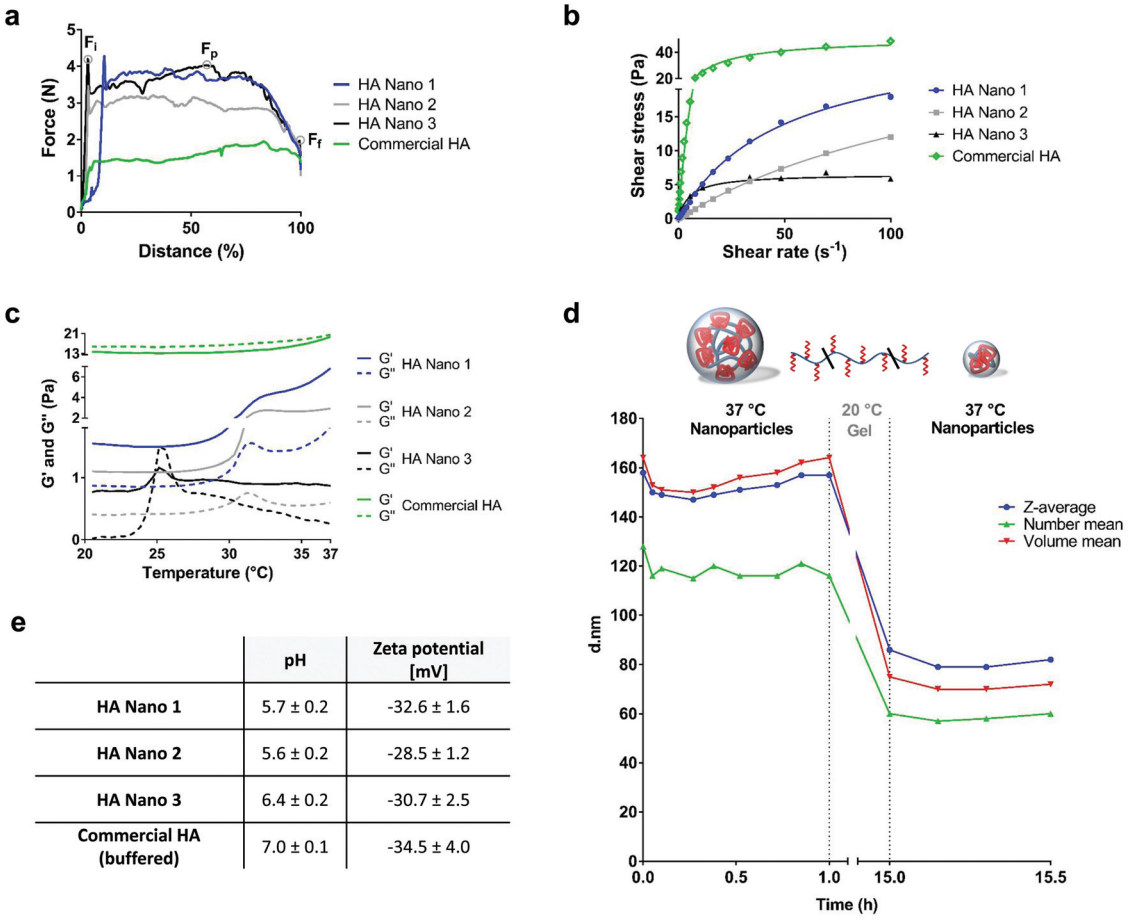

e

	pH	Zeta potential [mV]
HA Nano 1	5.7 ± 0.2	-32.6 ± 1.6
HA Nano 2	5.6 ± 0.2	-28.5 ± 1.2
HA Nano 3	6.4 ± 0.2	-30.7 ± 2.5
Commercial HA (buffered)	7.0 ± 0.1	-34.5 ± 4.0

Fig. 2 *In vitro* characterization of the HA conjugates: injectability, rheology and enzymatic degradation of the hydrogels and nanoparticles. a, Force in Newtons (N) required to expel the hydrogel at a maximum concentration close to the solubility limit (HA Nano 1, 2 and 3: 0.75, 0.5 and 5% (w/v), respectively) as a function of the stroke distance of the piston in a syringe with a 23G needle (distance %) at 20 °C. Three forces were assessed to characterize the injection profile: F_i (initial force), F_p (plateau force) and F_f (final force). b, Rheological behavior at 20 °C. c, Temperature dependence of the storage/elastic modulus (G') and the loss/viscosity modulus (G'') of the hyaluronic acid-based hydrogel conjugates. d, Representative enzymatic degradation (HA Nano 2: 0.1% (w/v): hyaluronidase 55 U mL^{-1} in PBS). e, pH and zeta potential (±s.d.) of the hydrogels in distilled water.

analyses, formulations HA Nano 1–2 were selected for their viscosities, which were closer to those of viscosupplementation products. HA Nano 3 was discarded due to its insufficient viscosity above the LCST.

The stability and enzymatic degradation of the two remaining HA conjugates were then evaluated. The HA conjugates were slightly acidic (pH 5.6–6.4) and had negative zeta potentials, ensuring colloidal stability (Fig. 2e). The stabilities of HA Nano 1–2 were evaluated for 1 month at 4 °C based on the viscosity changes at 100 s^{-1} and 20 °C (n = 3). The viscosities did not significantly change over one month, meaning that the stability of the hydrogels was maintained/preserved. The sensitivity to the enzymatic degradation of HA Nano 2 was assessed *in vitro* in the presence of high hyaluronidase concentrations (55 U mL^{-1} in PBS) (Fig. 2d) to evaluate the potential protecting effect of the nanoparticle architecture at body temperature. Above the LCST, the size of the nanoparticles did not change during the first 1 h phase at 37 °C, which was attributed to the poor enzymatic accessibility of the HA chains. This protection may have been caused by the hydrophobic nanoparticle structure sterically impeding the cleavage of a high molecular weight HA. At 20 °C, this sterically enhanced protective effect was lost, leading to a decrease in the nanoparticle size with time (Fig. 2d). At body temperature, the cleared nanoparticles maintained their diameter, whereas the conventional HA hydrogel was cleaved, reducing its viscosity significantly over a very short period of time (Fig. S4†). The hydrophobic nanoparticle structure showed another potentially useful property: the ability to be loaded with hydrophobic drug substances (Fig. S5†). This observation highlights a new characteristic of the HA conjugate nanoparticles in addition to their lubrication properties: their ability to deliver drugs.

After the physicochemical characterization of the nanostructures, the compatibility of the HA derivatives with cells was assessed in a mitochondrial activity assay using human fibroblast-like synoviocytes exposed to the HA conjugates. The cell viability did not decrease with HA Nano 1 (1% (w/v)) or with HA Nano 2 (0.5% (w/v)) at the concentrations used for the *in vivo* trials (Fig. S6†).

In vivo analyses in mice: tissue persistence, biocompatibility and function in an OA model

The tissue persistence of thermosensitive HA Nano 1 and conventional HA was assessed by subcutaneous injection in healthy mice or intra-articular injection in model OA in mice (6 weeks of age). For these experiments, 0.1% (w/w) cyanine 5 (λ_{ex} 646 nm, λ_{em} 662 nm) was covalently bound to thermosensitive HA Nano 1 and conventional HA. The persistence of the compounds was monitored for 21 days by semi-quantitative intravital fluorescence imaging using a Maestro M1 system (Fig. 3a–d). The residence time was defined as the time required to increase the fluorescent area by 20% relative to the area at day 0. Remarkably, the residence time of HA Nano 1 in the body exceeded 21 days near the injection site, a particular feature attributed to the spontaneous nanoparticle formation and observed for both intra-articular and subcutaneous injections (Fig. 3a and c). In contrast, HA diffused rapidly from the injection sites already at day 0. Approximately 1 h after injection, the spots of HA were larger than the areas of HA Nano 1. Then, HA was almost entirely cleared by day 21 from the initial injection site, reflecting the body clearance for both routes of administration (Fig. 3b and d). The presence of fluorescent HA and HA Nano 1 could still be observed in the paraffin-embedded tissue sections of the knee joints and the skin specimens (Fig. 3e and f). After intra-articular injection, the fluorescence of HA was mainly detected in the synovial tissue and only few particles in the bone marrow, in line with previous reports (Fig. S7†).[23] The results for HA Nano 1 were similar except for the higher fluorescence level remaining at the injection site. Most of the HA Nano 1 material was detected locally in the intra-articular capsule (Fig. 3e) or at the site of subcutaneous injection (Fig. 3f), which was different from HA. For both materials, HA diffused far away from the injection site and ultimately disappeared. This experiment confirmed the tissue persistence of HA Nano 1 in joints for at least 2 months after the first injection.

The skin biocompatibility of HA and HA Nano 1 was investigated in mice at 7 and 21 days following subcutaneous injection. The histological examination of the injected skin areas in H&E-stained sections demonstrated an average minimal inflammatory activity at all time points in all treatment groups (Fig. 4a). If inflammatory cells were present, they consisted – as assessed by the morphology – mainly of macrophages (some of them with foamy cytoplasm). Few macrophages were observed in the inflammatory reaction, similar to the commercial HA control (Fig. 4b). The observed empty spaces left in the dermis architecture were consistent with the presence of HA Nano 1 detected by fluorescence imaging (Fig. 3f).

To functionally evaluate the effects of HA Nano 1 application *in vivo* in mice, we utilized the surgical destabilization of the medial meniscus (DMM) as a dynamical mechanical model resembling chronic human OA. In all experimental groups, fluorescent HA and HA Nano 1 were injected intra-articularly on days 7 and 35 after surgery. The treatment groups were evaluated at day 63, two months after OA induction, for cartilage degradation/joint damage by histological analysis of SOFG stained tissue sections (Fig. 4c). The OARSI scores[21] demonstrated significant histological improvement of the medial joint halves of the right knee by HA and HA Nano 1 treatment compared to the PBS-treated control group (Fig. 4d). Medium OA (maximum grade detected: 4) without treatment was observed, with in-depth erosion or clefts of the calcified cartilage that extended to 25–50% of the articular surface. The lateral parts of the right knee were unaffected and served as an internal negative control, *i.e.* no lesion was present. The femoral and tibial knee cartilages treated with HA and HA Nano 1 were protected from mechanical damage due to their lubricating and shock-absorbing properties.[24] The percentage ratio of the medial/lateral tibial epiphysis thickness, which is the most relevant OA lesion region, was measured using micro-CT images. The cushioning effects and intra-articular persistence of HA Nano 1 tended to protect the medial epiphy-

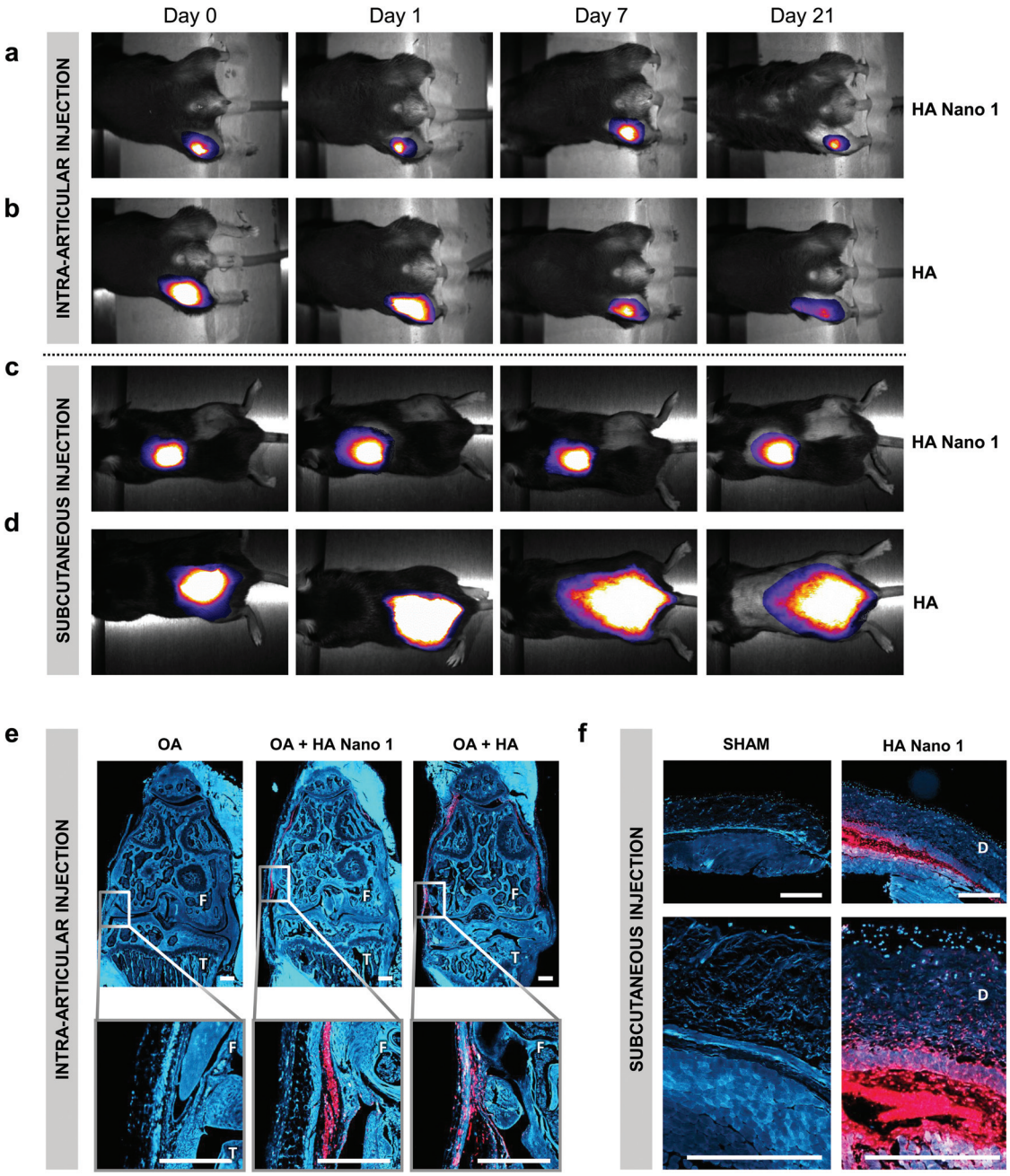

Fig. 3 Comparison of the tissue persistence of conventional HA (1% (w/v)) and thermosensitive HA Nano 1 (1% (w/v)) tagged with a covalently bound cyanine 5 dye. Representative figures of an intravital fluorescence superimposed with white light images in mice from day 0 (*ca.* 1 hour after injection) up to 21 days after a, b, intra-articular injection in an osteoarthritis (OA) mouse model (n = 7, injection volume: 10 μL) and c, d, subcutaneous injection in healthy mice (n = 4, injection volume: 100 μL). Fluorescence scale from purple to white including saturation. Identical image processing. Representative unstained paraffin-embedded tissue fluorescence micrographs at two magnifications (top, bottom) of e, right knee (frontal section of the destabilized knee; F: femur, T: tibia; scale bar = 300 μm) 2 months after OA induction and f, the skin at 21 days after injection (from top: epidermis, D: dermis, subcutaneous tissue and muscle; scale bar = 500 μm), autofluorescence of tissues (blue), and fluorescence of HA and HA Nano 1 (red). The sham group: mice received an injection of PBS.

sis probably by avoiding compression, resulting in a significantly higher epiphysis thickness than that in the HA group (Fig. 4e). The OA biomarker levels in mouse plasma were quantified using multiplex ELISA to assess the disease progression in the experimental groups. HA Nano 1 and HA inhibited VEGF, which plays a key role in cartilage degradation (Fig. 4f).[25] Furthermore, even though the DMM model is not an inflammatory model, HA Nano 1 reduced the level of inflammatory cytokines (IL-1β and TNFα), which were not significantly different from those in the sham group for both treatments (Fig. 4g and h). Taken together, these data indicate that the observed bioactivity of HA Nano 1 should reduce/slow

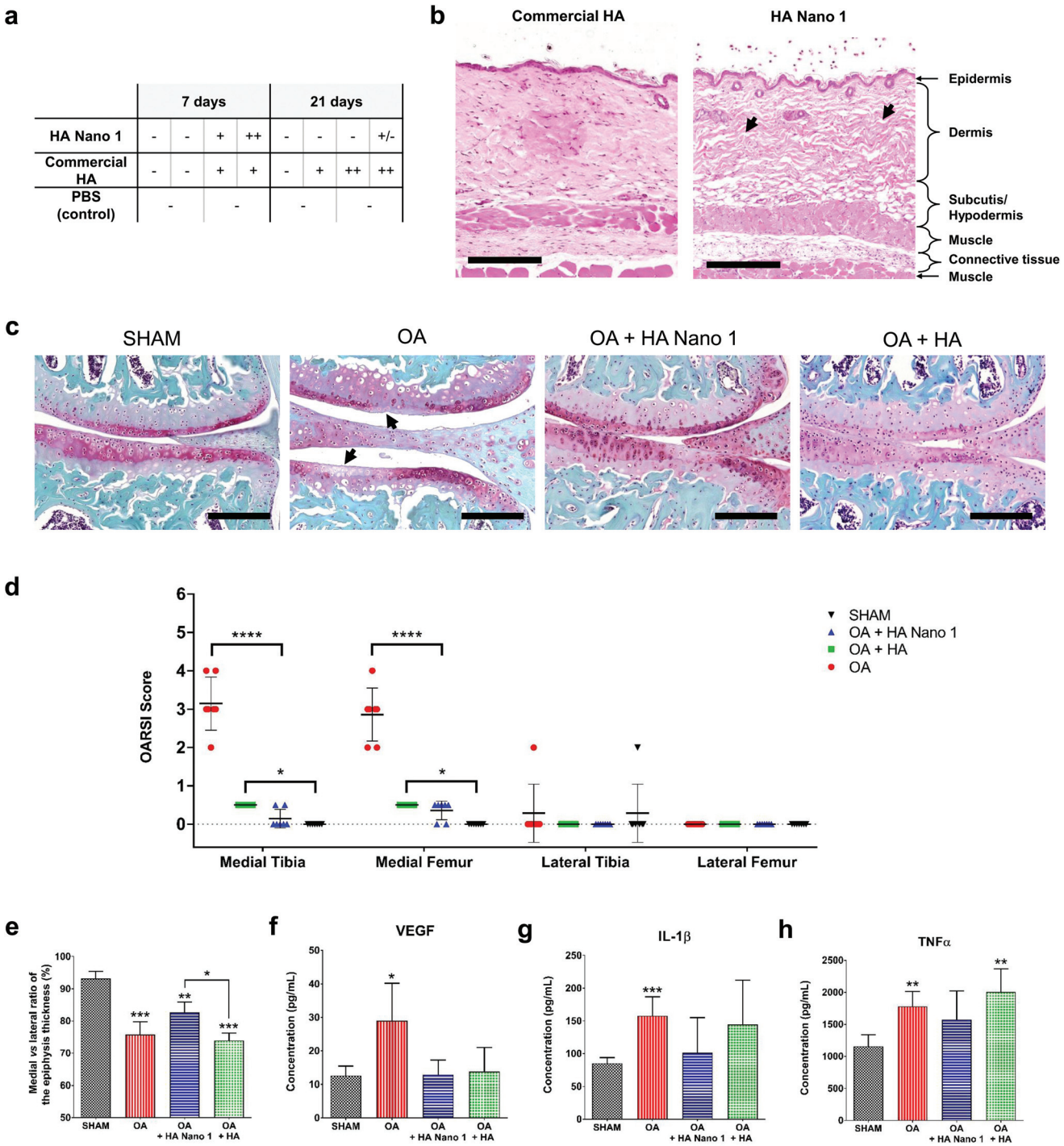

Fig. 4 *In vivo* biocompatibility (n = 2–4 per group) and bioactivity (n = 7 per group) studies. a, Biocompatibility of the polymers evaluated by semi-quantitative histological scoring after subcutaneous injection of 100 µL of the formulations into healthy mice. Semi-quantification of macrophages in the tissue based on histology from (–) to (+++). b, Representative optical micrographs of hematoxylin and eosin (H&E)-stained skin tissue sections, 21 days after subcutaneous injection. Arrows indicate empty spaces left in the dermis. Scale bar = 250 µm. c, Representative photomicrographs of Safranin-O/Fast Green (SOFG) stained articular sections of the medial right knee (destabilized) 2 months after surgery. Femur (top), tibia (low), and cartilage (stained in purple). Arrows indicate cartilage thinning/erosion. Scale bar = 200 µm. d, Comparison of histological OARSI scores of the medial femur/tibia (destabilized) to the lateral femur/tibia (untreated control) according to treatment groups from normal (0) to severe (6). e, Percentage ratio of medial/lateral tibial epiphysis at 2 months after the destabilization of the medial meniscus in mice measured from 3D micro-computed tomography (micro-CT) images. The multiplex ELISA analysis of f, vascular endothelial growth factor (VEGF) and the pro-inflammatory cytokines g, interleukin-1β (IL-1β) and h, tumor necrosis factor-α (TNFα) in the total plasma of mice at 2 months after OA induction. The data are presented as the mean ± s.d. *P < 0.0332, **P < 0.0021, ***P < 0.0002, and ****P < 0.0001 *versus* the sham group after ANOVA and Dunnett's test.

OA progression. These *in vivo* results support the idea that HA Nano 1 may serve as a novel visco-supplementation therapy for OA. Additionally, these HA Nano formulations have properties, such as slow degradation and higher residence time, suitable for dermatological and surgical applications.

Conclusions

In this study, we synthesized HA conjugates that spontaneously formed nanoparticles after injection at body temperature. HA Nano 1, a branched polymer of pNiPAM grafted to an HA backbone with appropriate linkers, is an easily injectable, stable, biocompatible and biodegradable material with a significantly prolonged residence time at the injection site compared to conventional HA. Besides, HA Nano 1 is less sensitive to hyaluronidase degradation than HA. HA Nano 1 has a protecting effect on the epiphysis thickness of the medial tibia, reducing VEGF, IL-1β, and TNFα, as shown in an OA mouse model, and can potentially be used as a drug delivery system for peptides, proteins or small molecules. Finally, this technology introduces the concept of self-lubricating nano-ball bearings as a new way of lubricating joints and various tissues in medical, surgical and cosmetic applications.

Conflicts of interest

There are no conflicts to declare.

Acknowledgements

The authors thank Professor Cem Gabay for his participation and help for the *in vitro* trials.

References

1 L. Klouda and A. G. Mikos, *Eur. J. Pharm. Biopharm.*, 2008, **68**, 34–45.
2 R. Stern, *Eur. J. Cell Biol.*, 2004, **83**, 317–325.
3 M. Lavertu, D. Filion and M. D. Buschmann, *Biomacromolecules*, 2008, **9**, 640–650.
4 J. R. Fraser, T. C. Laurent and U. B. Laurent, *J. Intern. Med.*, 1997, **242**, 27–33.
5 L. Robert, *Pathol. Biol.*, 2015, **63**, 32–34.
6 E. Papakonstantinou, M. Roth and G. Karakiulakis, *Dermatoendocrinol.*, 2012, **4**, 253–258.
7 T. J. Brown, U. B. Laurent and J. R. Fraser, *Exp. Physiol.*, 1991, **76**, 125–134.
8 Agency for Healthcare Research and Quality (US), *Comparative Effectiveness Review Summary Guides for Clinicians*, Rockville (MD), 2007.
9 C. E. Schante, G. Zuber, C. Herlin and T. F. Vandamme, *Carbohydr. Polym.*, 2011, **85**, 469–489.
10 H. G. Schild, *Prog. Polym. Sci.*, 1992, **17**, 163–249.
11 H. P. Tan, C. M. Ramirez, N. Miljkovic, H. Li, J. P. Rubin and K. G. Marra, *Biomaterials*, 2009, **30**, 6844–6853.
12 M. A. Cooperstein and H. E. Canavan, *Biointerphases*, 2013, **8**, 19.
13 Z. Q. Li and J. J. Guan, *Expert Opin. Drug Delivery*, 2011, **8**, 991–1007.
14 B. Jeong, S. W. Kim and Y. H. Bae, *Adv. Drug Delivery Rev.*, 2002, **54**, 37–51.
15 C. L. He, S. W. Kim and D. S. Lee, *J. Controlled Release*, 2008, **127**, 189–207.
16 F. Kohori, K. Sakai, T. Aoyagi, M. Yokoyama, Y. Sakurai and T. Okano, *J. Controlled Release*, 1998, **55**, 87–98.
17 S. Ohya, Y. Nakayama and T. Matsuda, *Biomacromolecules*, 2001, **2**, 856–863.
18 D. Mortisen, M. Peroglio, M. Alini and D. Eglin, *Biomacromolecules*, 2010, **11**, 1261–1272.
19 M. Peroglio, S. Grad, D. Mortisen, C. M. Sprecher, S. Illien-Junger, M. Alini and D. Eglin, *Eur. Spine J.*, 2012, **21**(Suppl. 6), S839–S849.
20 S. S. Glasson, T. J. Blanchet and E. A. Morris, *Osteoarthritis Cartilage*, 2007, **15**, 1061–1069.
21 S. S. Glasson, M. G. Chambers, W. B. Van Den Berg and C. B. Little, *Osteoarthritis Cartilage*, 2010, **18**(Suppl. 3), S17–S23.
22 F. Cilurzo, F. Selmin, P. Minghetti, M. Adami, E. Bertoni, S. Lauria and L. Montanari, *AAPS PharmSciTech*, 2011, **12**, 604–609.
23 N. Hiraoka, K. A. Takahashi, Y. Arai, K. Sakao, O. Mazda, T. Kishida, K. Honjo, S. Tanaka and T. Kubo, *J. Orthop. Res.*, 2011, **29**, 354–360.
24 G. Kogan, L. Soltes, R. Stern and P. Gemeiner, *Biotechnol. Lett.*, 2007, **29**, 17–25.
25 M. Murata, K. Yudoh and K. Masuko, *Osteoarthritis Cartilage*, 2008, **16**, 279–286.